

Electrostatic deflectors and dispersion suppressors: Their formulation and application to a storage ring

Masahiro Ikegami, Yoshihisa Iwashita, Hikaru Souda, Mikio Tanabe, and Akira Noda

Institute for Chemical Research, Kyoto University, Gokasho Uji, Kyoto 611-0011, Japan

(Received 11 March 2005; published 27 December 2005)

A single particle dynamics in beam bending elements including electrostatic fields is formulated. A general form of scalar potentials of electrostatic deflectors is obtained from solutions of the Maxwell equation having axial symmetry. Equations of motion of a charged particle in various types of the electrostatic deflectors are derived based on Hamiltonian formalism. The equation of motion in dispersion suppressors, which are a combination of the electrostatic deflectors and dipole magnets, are also formulated and generalized. Application of one of the dispersion suppressors to an existing heavy ion storage ring S-LSR provides the better condition for generation of a multidimensional crystalline beam. It is shown that this condition is achievable by real fabricated devices composed of a dipole magnet and an electrostatic deflector equipped with intermediate electrodes. The effectiveness of this dispersion suppressor for the real operation is shown by a particle tracking including the nonlinear field component.

DOI: [10.1103/PhysRevSTAB.8.124001](https://doi.org/10.1103/PhysRevSTAB.8.124001)

PACS numbers: 29.20.Dh, 41.20.Cv, 29.27.-a, 41.85.Lc

I. INTRODUCTION

In recent years, molecular dynamics (MD) studies showed that when a beam circulating in a storage ring is strongly cooled, the phase transition of the beam is expected [1,2]. The phase transition to a crystalline beam state occurs, if the ring has operating points satisfying so-called *crystal formation and maintenance conditions* [3,4], and a strong three-dimensional cooling force [5,6] is applied. The formation condition is that the Lorentz factor of the beam must be below the transition energy $\gamma_0 < \gamma_t$. The maintenance condition is that the ring must have operating points below the betatron tune of the value $N/2\sqrt{2}$, where N is the superperiodicity of the ring. Many advanced MD simulations have shown the creation of the crystalline beams in realistic storage ring models [2–4,6–8], when the above conditions are satisfied. On the other hand, it has also been known that the creation of a crystalline beam which has many particles is difficult without an ideal tapered cooling force [9] because of the *shear* heating induced by the dispersion [10]. It has been suggested that a storage ring constructed by a bending element simultaneously using electric field and magnetic field can eliminate the shear [11]. This element also can eliminate the linear dispersion of the beam [12,13], together with the shear [14]. Therefore such deflector is called a *dispersion suppressor*. In a (linear) dispersion-free storage ring constructed with the dispersion suppressor, the stability of the crystalline beam structure is thought to be greatly improved, even if the cooling force is not tapered.

At S-LSR [15], laser cooling experiment of a 35 keV, $^{24}\text{Mg}^+$ beam is to be performed, aiming at the generation of the ultimate-low-temperature beam, furthermore the creation of crystalline beam is also to be studied. The deflection elements of S-LSR are the dispersion suppressors constructed with a dipole magnet and a cylindrical electrostatic deflector.

S-LSR can operate as a conventional magnetic storage ring and a (linear) dispersion-free storage ring. S-LSR satisfies the formation and maintenance conditions for crystalline beams at the operation which uses only the magnetic field, although it requires a tapered cooling for the generation of multidimensional crystalline beams. In Ref. [14], the condition for crystalline beams in dispersion-free rings was investigated. It was found that the formation condition is satisfied in any dispersion-free storage ring, in principle. The maintenance condition is thought to be satisfied in a dispersion-free storage ring having the large number of lattice periods. However, in the case of the dispersion-free mode of S-LSR utilizing the cylindrical electrostatic deflector, there was no operating point satisfying the maintenance condition. It was found that the reason is the enhancement of the radial focusing induced by the electric field.

In this paper, in order to overcome this problem we take notice of the structure of the electrostatic deflector. Various structure of electrostatic deflector is possible and they have different focusing effects on beams in the deflector [16–19]. In Ref. [11], it was suggested that the focusing effect of the dispersion suppressor can be changed, if the field distribution of the electrostatic deflector or bending magnet is changed. The electrostatic potentials of the electrostatic deflectors used to derive the equation of motion must be the right solutions of Maxwell equation. Thus, in Sec. II, we carefully derived the general form of electrostatic potential from the Maxwell equation. Using this electrostatic potential, the linear equation of motion of a charged particle in the electrostatic deflector is derived. Furthermore, dispersion suppressors having a uniform magnetic field and the general electrostatic field are considered, and the single particle equation of motion in the dispersion suppressors is derived. In Sec. III, using the formula of Sec. II, the beam dynamics at S-LSR is investigated. It is shown that the

beam dynamics at S-LSR is greatly changed, when a different type of dispersion suppressor is introduced. Especially, when a dispersion suppressor having an electric field of the field index 0 is introduced, S-LSR becomes to have operating points satisfying the maintenance condition for crystalline beam. In Sec. IV, a practical method to realize the electric field for such dispersion suppressor is shown. From the third-order Hamiltonian, a second-order transport equation [20] of dispersion suppressor for tracking charged particle is derived. A particle tracking including the nonlinear field component of the dispersion suppressor is performed and the dynamic aperture is calculated. Using this result, the nonlinear effect on the crystalline beam, and the beam current needed for the experiment generating multidimensional crystalline beam are discussed.

II. ELECTROSTATIC DEFLECTORS AND DISPERSION SUPPRESSORS

A. Scalar potential of electrostatic deflectors

A strict formula of the scalar potential of electrostatic deflectors is derived in order to formulate the single particle dynamics in deflection elements including electrostatic fields. In accelerator physics, the Frenet-Serret coordinate system is usually used [21]. In this coordinate system, x and y describe the horizontal and the vertical position

$$\begin{aligned} \phi_D(x, y) = & A_{00} + A_{10} \left(x - \frac{y^2}{2\rho_0} + \frac{xy^2}{2\rho_0^2} - \frac{x^2y^2}{2\rho_0^3} + \frac{y^4}{24\rho_0^3} + \dots \right) + A_{20} \left(\frac{x^2}{2} - \frac{y^2}{2} - \frac{xy^2}{2\rho_0} + \frac{x^2y^2}{2\rho_0^2} - \frac{y^4}{24\rho_0^2} + \dots \right) \\ & + A_{30} \left(\frac{x^3}{6} - \frac{xy^2}{2} - \frac{x^2y^2}{4\rho_0} + \frac{y^4}{12\rho_0} + \dots \right) + A_{40} \left(\frac{x^4}{24} - \frac{x^2y^2}{4} + \frac{y^4}{24} + \dots \right) + \dots \end{aligned} \quad (2)$$

The electric field component on the reference orbit is

$$E_x(0, 0) = - \left. \frac{\partial \phi_D}{\partial x} \right|_{\substack{x=0 \\ y=0}} = -A_{10} \quad E_y(0, 0) = - \left. \frac{\partial \phi_D}{\partial y} \right|_{\substack{x=0 \\ y=0}} = 0. \quad (3)$$

Therefore, A_{10} decides the strength of the bending effect. In the following, the coefficients of Eq. (2) are supposed to be $A_{00} = 0$, $A_{10} = V_0/\rho_0$, $A_{n0} = K_{n-1}V_0/\rho_0^n$.

Furthermore, we define the field index of the bending electric field by

$$n = - \left. \frac{\rho_0}{E_x} \frac{\partial E_x}{\partial x} \right|_{\substack{x=0 \\ y=0}}. \quad (4)$$

When these coefficients are substituted to Eq. (2), the potential becomes

$$\begin{aligned} \phi_D(x, y) = & V_0 \left\{ \left[\frac{x}{\rho_0} - \frac{1}{2} \left(\frac{y}{\rho_0} \right)^2 + \frac{1}{2} \left(\frac{x}{\rho_0} \right) \left(\frac{y}{\rho_0} \right)^2 - \frac{1}{2} \left(\frac{x}{\rho_0} \right)^2 \left(\frac{y}{\rho_0} \right)^2 + \frac{1}{24} \left(\frac{y}{\rho_0} \right)^4 + \dots \right] \right. \\ & - n \left[\frac{1}{2} \left(\frac{x}{\rho_0} \right)^2 - \frac{1}{2} \left(\frac{y}{\rho_0} \right)^2 - \frac{1}{2} \left(\frac{x}{\rho_0} \right) \left(\frac{y}{\rho_0} \right)^2 + \frac{1}{2} \left(\frac{x}{\rho_0} \right)^2 \left(\frac{y}{\rho_0} \right)^2 - \frac{1}{24} \left(\frac{y}{\rho_0} \right)^4 + \dots \right] \\ & + K_2 \left[\frac{1}{6} \left(\frac{x}{\rho_0} \right)^3 - \frac{1}{2} \left(\frac{x}{\rho_0} \right) \left(\frac{y}{\rho_0} \right)^2 - \frac{1}{4} \left(\frac{x}{\rho_0} \right)^2 \left(\frac{y}{\rho_0} \right)^2 + \frac{1}{12} \left(\frac{y}{\rho_0} \right)^4 + \dots \right] \\ & \left. + K_3 \left[\frac{1}{24} \left(\frac{x}{\rho_0} \right)^4 - \frac{1}{4} \left(\frac{x}{\rho_0} \right)^2 \left(\frac{y}{\rho_0} \right)^2 + \frac{1}{24} \left(\frac{y}{\rho_0} \right)^4 + \dots \right] + \dots \right\}. \end{aligned} \quad (5)$$

This form is useful to derive the equation of motion approximated in finite order.

deviations from the reference orbit, s is the arc length measured along the reference orbit from the reference initial point. The radius of the curvature of the reference orbit is denoted as ρ_0 . In the electrostatic deflector, the scalar potential is supposed to satisfy the following conditions. The first condition is the electrostatic potential has no s dependence. This means the reference particle is not accelerated in the direction of the movement. The electrostatic deflectors used in actual electrostatic storage rings, such as cylindrical and spherical electrostatic deflector [17–19,22,23], satisfy this condition. This condition simplifies the treatment of the electrostatic deflector in the optics calculation, since the kinetic energy of the reference particle conserves. The second condition is that the electrostatic potential should be symmetric about y . This condition means the electrostatic deflector has a structure symmetric about the median plane.

When the scalar potential is expressed in a power series of particle coordinates [24,25],

$$\phi_D = \sum_{i,j>0} A_{ij} \frac{x^i}{i!} \frac{y^j}{j!}, \quad (1)$$

the coefficients are decided from the Laplace equation and the above conditions. Substituting Eq. (1) into the Laplace equation, and imposing the symmetry condition, the scalar potential of electrostatic deflectors becomes

If one needs a complete solution, not expanded form, one can obtain it by solving the Maxwell equation directly (see Appendix A). This method leads the complete form of the electrostatic potentials for the spherical, cylindrical, and hyperboloidal electrostatic deflector, etc. Of course, the power expansions of these electrostatic potentials become the form of Eq. (5).

B. Single particle dynamics in electrostatic deflectors

In this section, the single particle dynamics in electrostatic deflectors is formulated by using the general electrostatic potential [Eq. (5)]. The Frenet-Serret coordinate system used in the previous section is utilized. The charged particle is supposed to be bent with the bending radius ρ_0 . Since the electric field strength is V_0/ρ_0 along the design orbit, the equilibrium reference momentum becomes

$$p_0 = \frac{qV_0}{\beta_0 c}, \quad (6)$$

where β_0 is the velocity of the reference particle divided by light speed c .

When the path length s is selected as the independent variable, the relativistic Hamiltonian which governs the motion of a charged particle in a bending electric field and a magnetic field is given by [26]

$$H = -\left(1 + \frac{x}{\rho_0}\right) \sqrt{\left(\frac{p_t + q\phi_D}{c}\right)^2 - m^2 c^2 - p_x^2 - p_y^2} - q\left(1 + \frac{x}{\rho_0}\right) A_s, \quad (7)$$

where m and q are the rest mass and charge state of particles, respectively, ϕ_D is the scalar potential of the electrostatic deflector, A_s is the s component of the vector potentials of bending magnets, p_t is the canonical momentum conjugate to time t . p_t relates to the energy of the particle by a relation $p_t = -E$. When the canonical momentum is redefined by

$$\frac{\Delta E}{c p_0} = \frac{E}{c p_0} - \frac{1}{\beta_0}, \quad (8)$$

using the relative time $-c\Delta t = ct_0 - ct$ and the Hamiltonian is divided by the reference momentum p_0 , it is transformed to

$$\begin{aligned} \tilde{H} &= \frac{1}{\beta_0} \frac{\Delta E}{c p_0} - \left(1 + \frac{x}{\rho_0}\right) \\ &\times \sqrt{1 + \frac{2}{\beta_0} \left(\frac{\Delta E - q\phi_D}{c p_0}\right) + \left(\frac{\Delta E - q\phi_D}{c p_0}\right)^2 - \tilde{p}_x^2 - \tilde{p}_y^2} \\ &- \left(1 + \frac{x}{\rho_0}\right) \frac{q A_s}{p_0}, \end{aligned} \quad (9)$$

where the first term of the right-hand side has arisen since the canonical variables (t, p_t) have been changed to $(-c\Delta t, \Delta E/c p_0)$ (see Appendix B). The Hamiltonian has been divided by p_0 , and the transverse momenta have been normalized to be dimensionless; namely, $\tilde{p}_{x(y)} = p_{x(y)}/p_0$. In the case of the electrostatic deflectors, $A_s = 0$. Substitution of the scalar potential Eq. (5) and the equilibrium condition Eq. (6), expansion of the square root, and leaving up to second-order terms of the canonical variables leads the approximated Hamiltonian of the electrostatic deflectors

$$\begin{aligned} \tilde{H} &\approx \frac{1}{2\gamma_0^2} \left(\frac{\Delta E}{\beta_0^2 E_0}\right)^2 + \frac{\tilde{p}_x^2 + \tilde{p}_y^2}{2} - \frac{1}{2} \left(n - \frac{1}{\gamma_0^2} - 2\right) \left(\frac{x}{\rho_0}\right)^2 \\ &- \frac{1}{2} (1 - n) \left(\frac{y}{\rho_0}\right)^2 - \left(1 + \frac{1}{\gamma_0^2}\right) \frac{x}{\rho_0} \frac{\Delta E}{\beta_0^2 E_0}, \end{aligned} \quad (10)$$

where γ_0 is the Lorentz factor of the reference particle; $\gamma_0 = (\sqrt{1 - \beta_0^2})^{-1}$, the constant term has been neglected. From this Hamiltonian, the linear equations of motion for a set of canonical variables $(x, \tilde{p}_x, y, \tilde{p}_y, -c\Delta t, \Delta E/c p_0)$ are obtained. Especially, the horizontal and the vertical equations of motion are

$$\frac{d^2 x}{ds^2} = -\left(2 + \frac{1}{\gamma_0^2} - n\right) \frac{x}{\rho_0^2} + \frac{1}{\rho_0} \left(1 + \frac{1}{\gamma_0^2}\right) \frac{\Delta E}{\beta_0^2 E_0}, \quad (11a)$$

$$\frac{d^2 y}{ds^2} = -(n - 1) \frac{y}{\rho_0^2}. \quad (11b)$$

From these equations, it is found that the focusing strength of the electrostatic deflectors is decided by the field index n . The field indices of the spherical, cylindrical, and hyperboloidal electrostatic deflector are listed in Table I. The possible value of the field index is an arbitrary real number. Various field indices are realized by the electrostatic potentials obtained from the Maxwell equation (see Appendix A) and their linear combinations. In nonrelativistic limit $\gamma_0 \rightarrow 1$, the second term of the right-hand side of Eq. (11a) becomes $1/\rho_0 \cdot \Delta W/W_0$, where W_0 is the kinetic

TABLE I. Field index of electrostatic deflectors.

Structure of electrostatic deflector	Spherical	Cylindrical	Hyperboloidal
Value of n	2	1	-1

energy of the reference particle, ΔW is the energy difference including the potential energy.

C. Single particle dynamics in dispersion suppressors

In this section, single particle dynamics in dispersion suppressors of the combination of a uniform magnetic field and the general electric field obtained in Sec. II A is investigated. The uniform magnetic field is generated by a flat pole dipole magnet. Then, the vector potential has the form

$$A_s = -\frac{B_y}{2}(\rho_0 + x), \quad (12)$$

where B_y is the magnetic flux density of the dipole magnet, the other components are 0 ($A_x = A_y = 0$). The direction of the electric field is the reverse to the case of electrostatic deflectors, in order to compensate the dispersion. Therefore, the scalar potential has a reverse sign to Eq. (5). Then, the condition of the equilibrium orbit is given by the relation

$$p_0 = qB_y\rho_0 - \frac{qV_0}{\beta_0 c}. \quad (13)$$

By the same way of the previous section, Hamiltonian (9) is expanded, and the vector potential Eq. (12), the scalar potential, and the equilibrium condition Eq. (13) are substituted. Finally, leaving up to second-order terms of the canonical variables and neglecting the constant term, the Hamiltonian becomes

$$\begin{aligned} \tilde{H} \approx & \frac{1}{2\gamma_0^2} \left(\frac{\Delta E}{\beta_0^2 E_0} \right)^2 + \frac{\tilde{p}_x^2 + \tilde{p}_y^2}{2} - \frac{\Delta E}{\beta_0^2 E_0} \frac{x}{\rho_0} \left(1 - \frac{qV_0}{\gamma_0^2 \beta_0^2 E_0} \right) \\ & + \frac{1}{2} \left[1 - (1-n) \frac{qV_0}{\beta_0^2 E_0} + \frac{1}{\gamma_0^2} \left(\frac{qV_0}{\beta_0^2 E_0} \right)^2 \right] \left(\frac{x}{\rho_0} \right)^2 \\ & + \frac{1}{2} (1-n) \frac{qV_0}{\beta_0^2 E_0} \left(\frac{y}{\rho_0} \right)^2. \end{aligned} \quad (14)$$

Then the transverse equations of motion are

$$\begin{aligned} \frac{d^2 x}{ds^2} = & - \left[1 - (1-n) \frac{qV_0}{\beta_0^2 E_0} + \frac{1}{\gamma_0^2} \left(\frac{qV_0}{\beta_0^2 E_0} \right)^2 \right] \frac{x}{\rho_0^2} \\ & + \frac{1}{\rho_0} \left(1 - \frac{qV_0}{\gamma_0^2 \beta_0^2 E_0} \right) \frac{\Delta E}{\beta_0^2 E_0}, \end{aligned} \quad (15a)$$

$$\frac{d^2 y}{ds^2} = -(1-n) \frac{qV_0}{\beta_0^2 E_0} \frac{y}{\rho_0^2}. \quad (15b)$$

The last term of Eq. (15a) is the origin of the linear dispersion. Therefore, if the relation $qV_0/\gamma_0^2\beta_0^2E_0 = 1$ is satisfied, the linear dispersion is canceled out. From this relation and the condition of equilibrium orbit Eq. (13), the relation $(1 + 1/\gamma_0^2)E_x(0,0) = \beta_0 c B_y$ is obtained, where $E_x(0,0)$ is the strength of the bending electric field on the reference orbit, i.e., $E_x(0,0) = V_0/\rho_0$. This condition is completely the same as the dispersion-free condition

shown in Ref. [14]. When the dispersion-free condition $qV_0/\gamma_0^2\beta_0^2E_0 = 1$ is imposed, the equations of motion become

$$\frac{d^2 x}{ds^2} = -(1 + n\gamma_0^2) \frac{x}{\rho_0^2}, \quad (16a)$$

$$\frac{d^2 y}{ds^2} = -\gamma_0^2(1-n) \frac{y}{\rho_0^2}. \quad (16b)$$

III. DISPERSION-FREE STORAGE RING

A. Deflectors for a dispersion-free storage ring

The dispersion-free storage ring can eliminate the shear, and it has a possibility to generate a crystalline beam which has finite horizontal extent, by a conventional cooling force. In this section, we choose the lattice parameters of S-LSR for the example of this paper.

We reported the beam dynamics in a dispersion-free storage ring S-LSR constructed with the cylindrical dispersion suppressor of the field index 1 [14]. The result is that S-LSR cannot operate satisfying the maintenance condition for crystalline beam due to the strong radial focusing of the cylindrical dispersion suppressor. This dispersion suppressor has the focusing effect only in the horizontal (radial) directions. On the other hand, Eqs. (16) show the dispersion suppressor has the focusing effect in both directions, if the field index n is selected to the value between $-1/\gamma_0^2$ to 1. Especially, if the field index n is selected to $n = 0$, the deflector has almost the same focusing strength in both directions in the nonrelativistic limit. In this case, the radial focusing is suppressed compared with the cylindrical case. Since the radial focusing is suppressed, it is expected that the betatron tune is reduced without changing the basic structure of the lattice.

B. Transfer matrix calculation

The betatron tune of the dispersion-free mode of S-LSR is investigated when the dispersion suppressor which has a focusing effect in both horizontal and vertical directions is introduced. In this section, the value of the field index is supposed to be $-1/\gamma_0^2 < n < 1$. The lattice parameters are obtained by the transfer matrix calculation, by the same way as Ref. [14]. The transfer matrix acts on the phase space coordinates $(x, \tilde{p}_x, y, \tilde{p}_y, -c\Delta t, \Delta E/c\rho_0)$ [27]. When the following notation

$$\begin{aligned} k_x = \frac{\sqrt{1+n\gamma_0^2}}{\rho_0} \quad k_y = \frac{\gamma_0\sqrt{1-n}}{\rho_0} \quad C_x = \cos k_x L \\ S_x = \sin k_x L \quad C_y = \cos k_y L \quad S_y = \sin k_y L \end{aligned} \quad (17)$$

is introduced, the linear transfer matrix of the dispersion suppressor becomes

$$R_{ij} = \begin{pmatrix} C_x & S_x/k_x & 0 & 0 & 0 & 0 \\ -k_x S_x & C_x & 0 & 0 & 0 & 0 \\ 0 & 0 & C_y & S_y/k_y & 0 & 0 \\ 0 & 0 & -k_y S_y & C_y & 0 & 0 \\ 0 & 0 & 0 & 0 & 1 & \frac{L}{\beta_0^2 \gamma_0^2} \\ 0 & 0 & 0 & 0 & 0 & 1 \end{pmatrix}, \quad (18)$$

under the dispersion-free condition, where L is the orbit length of the reference particle in the deflector. From the linear transfer matrix, the lattice parameters of S-LSR can be calculated. In the following we select the field index to 0. The specifications of S-LSR are shown in Table II, the structure of the lattice period is shown in Fig. 1.

For the lattice of S-LSR utilizing the dispersion suppressor of the field index 0, the stable region of the betatron oscillation becomes as shown in Fig. 2. The characteristic of this stable region is that the beam can be circulated stably without quadrupole magnet. This is the result from that the deflection element has the focusing effect in both directions. This lattice enables us to operate the ring, satisfying the maintenance condition for crystalline beams. For example, the betatron tune of the value $(\nu_x, \nu_y) = (2.072, 2.072)$ is possible and the strength of the quadrupole magnets to realize this tune value is $(k_1, k_2) = (0.78[\text{m}^{-2}], -1.24[\text{m}^{-2}])$. In this operating point, the strength of the quadrupole magnets is very weak compared to the case using the cylindrical electric field [14], since the focusing force of the deflector is dominant. The beta functions in the lattice period become as shown in Fig. 3. Since this operating point satisfies the maintenance condition; $\max(\nu_x, \nu_y) < N/2\sqrt{2}$, if an adequate strong three-dimensional cooling force induced by a coupling cavity [5,7] is available, beam crystallization is expected to be realized at the dispersion-free mode of S-LSR.

IV. EVALUATION FOR THE REAL OPERATION

A. Generation of an actual electric field

From Eq. (5), on the median plane, the electric field of the dispersion suppressor is described as

$$E_x(x, 0) = \frac{V_0}{\rho_0} \left(1 - n \frac{x}{\rho_0} + \frac{K_2}{2!} \left(\frac{x}{\rho_0} \right)^2 + \frac{K_3}{3!} \left(\frac{x}{\rho_0} \right)^3 + \dots \right). \quad (19)$$

TABLE 2. Main parameters of S-LSR (Storage of $^{24}\text{Mg}^+$)

Quantity	Value
Cooled ion species	$^{24}\text{Mg}^+$
Kinetic beam energy	35 keV
Ring circumference	22.557 m
Radius of curvature at the bending section	1.05 m
Number of lattice periods	6

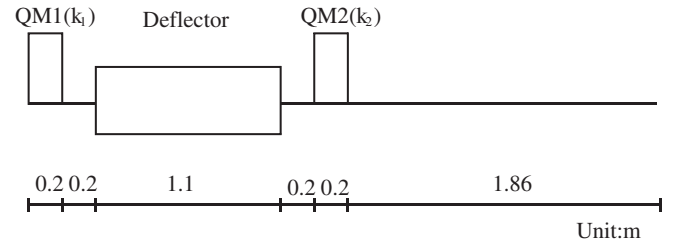


FIG. 1. The structure of the lattice period of S-LSR. The deflector can be used as both a dipole magnet and a dispersion suppressor. k_1 and k_2 are the values of the field gradient of the quadrupole magnets.

Note that the direction of the electric field is reversed to the case of electrostatic deflector. It is found that the electric field of the field index $n = 0$ has approximately radially uniform field distribution near the reference orbit ($x/\rho_0 \ll 1$). One of the methods to generate such an electric field is to use the electrostatic potential which is the linear combination of the cylindrical ($n = 1$) and the hyperboloidal ($n = -1$) electrostatic potential. The electrostatic deflector will be constructed with two electrodes placed in the different two equal potential surfaces (see Appendix A). However, this method needs electrodes having a complex shape. At S-LSR, cylindrical electrostatic deflectors equipped with intermediate electrodes are introduced [28]. The intermediate electrodes were introduced for the purpose maintaining the field strength and distribution in the aperture (Fig. 4). Furthermore, the intermediate elec-

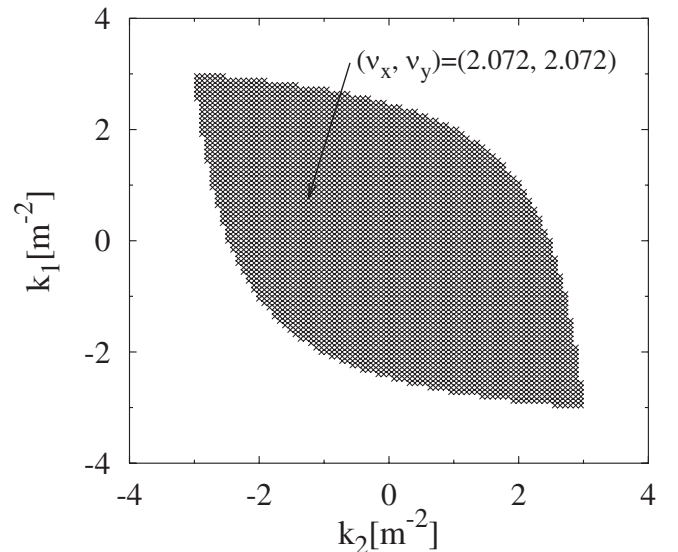


FIG. 2. Stable region of the linear betatron oscillation. The field gradient of two quadrupole magnets k_1 and k_2 are selected as the parameter. The minus sign of the field gradient means that the quadrupole magnet has a defocusing effect in the horizontal direction. The tune values at the operating point $(k_1, k_2) = (0.78[\text{m}^{-2}], -1.24[\text{m}^{-2}])$ are $(\nu_x, \nu_y) = (2.072, 2.072)$.

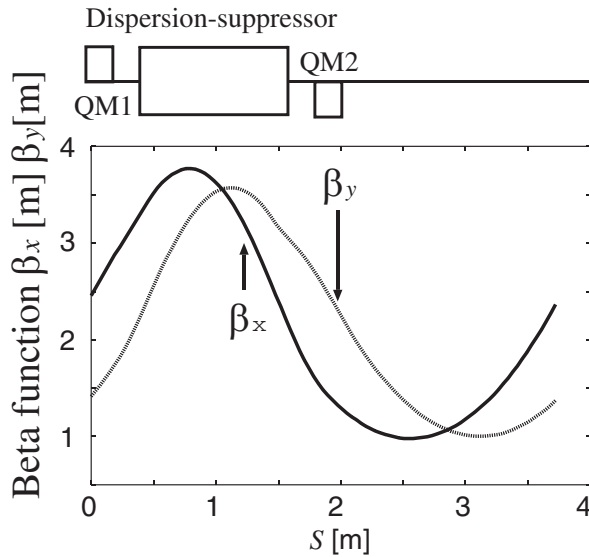


FIG. 3. Beta functions at the operating point $(k_1, k_2) = (0.78[\text{m}^{-2}], -1.24[\text{m}^{-2}])$, $(\nu_x, \nu_y) = (2.072, 2.072)$. The beta functions are drawn as a function of the position s .

trodes create a new possibility which realizes various field distributions in the electrostatic deflector. The voltage applied to the intermediate electrodes strongly dominates the electric field distribution in the electrostatic deflector. By using a field calculation code POISSON, we have confirmed that the field distributions of the field indices 1 and 0 can be generated near the reference orbit by adjusting the applied voltages to the intermediate electrodes [29]. Comparing the field distribution on the median plane obtained from the field calculation and Eq. (19), it was found that the coefficient of the higher-order term has a considerably large value. In the case of S-LSR, it is difficult to suppress the size of the coefficients of the higher-order term, because the height of the electrostatic deflector has been limited (Fig. 4) [30]. Therefore, strong nonlinearity is expected in the motion of particles passing through such electric field. In the next section, the nonlinearity of such dispersion suppressor is investigated.

B. Dynamic aperture calculation

1. Particle tracking including nonlinear effects

In the previous section, it has been suggested that various field indices of the electrostatic deflector are realized by a cylindrical electrostatic deflector equipped with the intermediate electrodes. However, this method may induce strong nonlinearity in the particle motion, for the case of S-LSR.

In order to investigate the nonlinear effects, particle tracking is performed by using the second-order transport equation [20]. For a phase space vector at the position s_0 $\mathbf{v}_i(s_0) = (x, \tilde{p}_x, y, \tilde{p}_y, -c\Delta t, \Delta E/cp_0)$, this equation gives a new phase space vector at the position s_1 by the following transformation

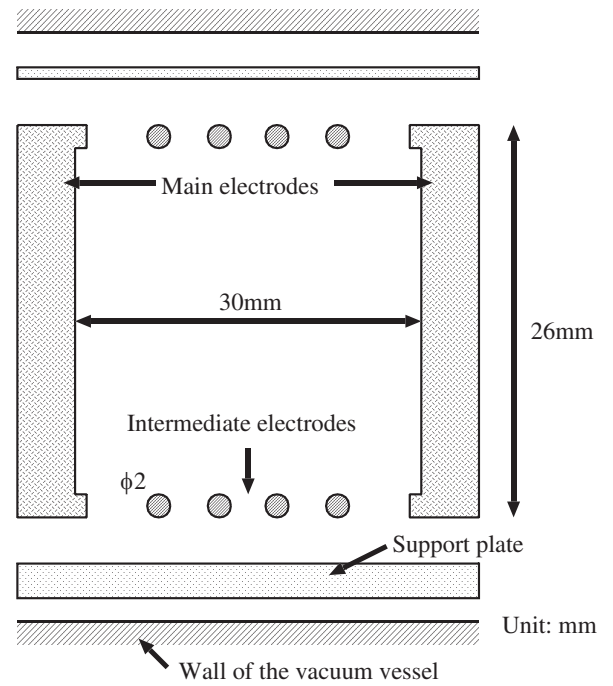


FIG. 4. Cross section around the electrostatic deflector of S-LSR. The height of the electrostatic deflector is limited by the gap size of the dipole magnet and the vacuum vessel. The electrostatic deflector is constructed with a pair of main electrodes and four pairs of intermediate electrodes. The voltage applied to the intermediate electrodes strongly dominates the electric field distribution in the electrostatic deflector. Therefore, various field distributions can be realized approximately by changing the applied voltage to the intermediate electrodes.

$$\mathbf{v}_i(s_1) = \sum_{j=1}^6 R_{ij} \mathbf{v}_j(s_0) + \sum_{j=1}^6 \sum_{k=1}^6 T_{ijk} \mathbf{v}_j(s_0) \mathbf{v}_k(s_0). \quad (20)$$

The first term of the right-hand side is the linear transformation by the transfer matrix R_{ij} , the second term gives the transformation by the nonlinear terms. The coefficients of the nonlinear terms T_{ijk} are given by the third-order Lie transformation obtained from the third-order Hamiltonian [20]. The third-order Hamiltonian, the derivation method of Lie transformation, and T_{ijk} for the dispersion suppressor are shown in Appendix C. In this section, the filed index of the dispersion suppressor is selected to 0, and the coefficient of the higher-order component of the electric field K_2 is estimated to be the order of 10 from the 2D field calculation by POISSON. The particle orbit is tracked during 3000 turns in the lattice of the dispersion-free mode of S-LSR including nonlinear effects.

2. Selection of the operating point

It is expected that the dynamic aperture of the dispersion suppressor of S-LSR is limited, since this includes nonlinear fields. It is well known that the dynamic aperture depends on the betatron tune. Thus, we investigate the tune

dependence of the dynamic aperture. When a strong non-linear field exists in the storage ring, the betatron tune depends on the amplitude of the betatron oscillation. This means the tunes of the particles in the beam are not identical. Therefore, in this paper, we select the linear tune (design tune) as the standard of the betatron motion. The design tune is uniquely determined by the lattice structure. When S-LSR is operated to generate crystalline beams, the design tune has to be below $(\nu_x, \nu_y) = (2.12, 2.12)$ from the requirement of the maintenance condition. On the other hand, it is expected that the beam cannot circulate stably near the integer tune $(\nu_x, \nu_y) = (2.0, 2.0)$. It has been found that the lower limit of the betatron tune is about $(\nu_x, \nu_y) = (2.0, 2.0)$ from the analyses of the linear betatron motion. Thus, the region to search an operating point having maximum dynamic aperture is limited to the range $2.04 < \nu_{x(y)} < 2.12$. The tune dependence of the on-momentum dynamic aperture at the center of the dispersion suppressor is plotted in the (ν_x, ν_y) plane (Fig. 5).

A dissipative force such as a laser cooling force acts on only one direction. In order to generate an ultimate-low-temperature beam, a three-dimensional cooling using a resonance coupling method [5,6] is essential. The resonance condition is given by the relation $\nu_x - \nu_s = \text{integer}$, $\nu_x - \nu_y = \text{integer}$, where ν_s is the synchrotron tune. Thus, it is better that the operating point place on the line $\nu_x = \nu_y$. On this line, dynamic aperture becomes large as the betatron tune approaches $(\nu_x, \nu_y) = (2.12, 2.12)$. However, in order to suppress the blocking of the beam cooling induced by second-order coherent resonances which originate in the machine lattice [31], it is better that the tune value is as low as possible. Thus, the operating point should be apart from $(\nu_x, \nu_y) = (2.12, 2.12)$ as far as possible. Eventually, we select the operating point $(\nu_x, \nu_y) = (2.072, 2.072)$, since this operating point has an adequate dynamic aperture, and is far from both the integer tune and the limit of the maintenance condition. The detailed configuration of the on-momentum dynamic aperture in the x - y plane at the operating point $(\nu_x, \nu_y) = (2.072, 2.072)$ is shown in Fig. 6.

C. Discussion for the experiment

We can estimate the maximum accumulable beam current from the result of the dynamic aperture calculation and the twiss parameters obtained from the transfer matrix calculation in Sec. III B. Using these parameters, the ring acceptance is estimated to be 3.31π mm mrad in the horizontal direction, and 2.71π mm mrad in the vertical direction. The 35 keV, $^{24}\text{Mg}^+$ beam pulled out from the ion source is injected to the ring during one turn by using an electric inflector. The maximum current of the beam which can be extracted from the ion source is estimated to be more than 0.4 mA, and its emittance is 40.5π mm mrad in

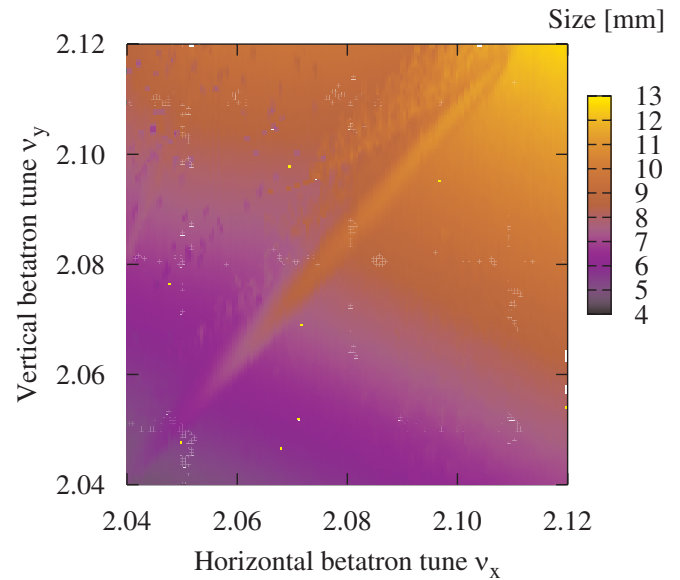


FIG. 5. (Color) Betatron tune dependence of on-momentum dynamic aperture of S-LSR, at the center of the deflector. The horizontal and the vertical axis are the horizontal and vertical linear tune. The color indicates the size of the dynamic aperture. The initial condition of the particles is $x = y$, the other canonical variables are 0. In this distribution map, the maximum value of $2\sqrt{xy}$, which the particle can circulate during 3000 turns is plotted at each operating point. In this tracking, individual error of the lattice element has not been considered; namely, the superperiodicity of the ring is completely 6.

both the horizontal and vertical directions. The small emittance part of the beam is selected by a x - y slit and injected to the ring. From the above parameters, the maximum current which can be accumulated in the ring is estimated to be $2.45 \mu\text{A}$.

Next, the beam current needed for the experiment generating crystalline beams is estimated. The line density of

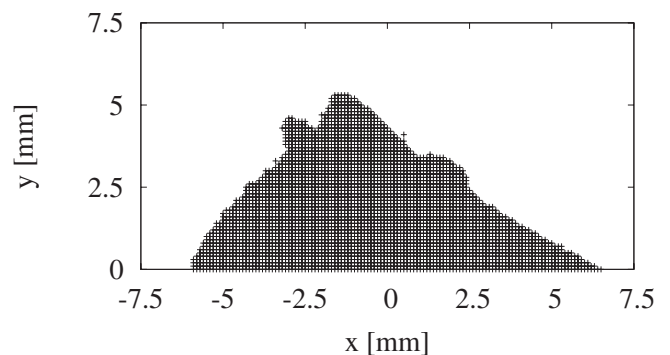


FIG. 6. The configuration of the on-momentum dynamic aperture in x - y plane, at the center of the deflector. This aperture has been calculated at the operating point $(\nu_x, \nu_y) = (2.072, 2.072)$. The horizontal dynamic aperture is not symmetric since the force driving the horizontal betatron motion is not symmetric about x .

the crystalline beams in storage rings can be approximately predicted from a Hasse-Schiffer's uniform confining field model [32]. As discussed in Sec. III, the focusing force of the dispersion-free mode of S-LSR is dominated by the dispersion suppressor, and its focusing force is almost equal in the horizontal and the vertical direction at the operating point $(\nu_x, \nu_y) = (2.072, 2.072)$. Therefore, the lattice structure of S-LSR is similar to this model. When the lattice of S-LSR is approximated with a smooth approximation, it is estimated that the crystalline beam structure changes to 2D state at the line density of $1.56 \times 10^4 [\text{m}^{-1}]$, and at the line density of $2.13 \times 10^4 [\text{m}^{-1}]$, the structure changes to 3D state. In the case of 35 keV, $^{24}\text{Mg}^+$ beam, these line densities correspond to the beam currents of 1.31 and 1.79 nA, respectively. Therefore, the ring can accumulate an enough current needed for the generation of multidimensional crystalline beam.

If the beam reaches to the crystalline state, the order of the beam size can be predicted from the Hasse-Schiffer's model. According to this model, the average volume which is occupied by a particle in crystalline beams is indicated by Wigner-Seitz radius. The Wigner-Seitz radius is decided by the strength of the confining field. In our case, this radius can approximately be obtained using the smooth approximation. The Wigner-Seitz radius at the operating point $(\nu_x, \nu_y) = (2.072, 2.072)$ is $4.53 \times 10^{-5} [\text{m}]$. For example, if a one-helix crystalline beam can be formed in the lattice of S-LSR, the radius of the helix is estimated to be 0.05 [mm]. Furthermore, if a 6-shell crystalline beam can be formed, the radius of the shell is estimated to be 0.38 [mm].

A dynamic aperture indicates the beam size where the nonlinear effect becomes dominant. Since the estimated sizes of the crystalline beams are far smaller compared to the size of the dynamic aperture, the effect of the nonlinear field component of the dispersion suppressor described in the previous section is considered to be negligible when the beams reach to crystalline state.

V. CONCLUSIONS

The beam dynamics in a dispersion-free storage ring has been investigated by using the general formula of deflection elements including electric fields. The dispersion suppressor of the field index 0 provides better focusing force for the operation of S-LSR aiming at the generation of crystalline beam. When such a dispersion suppressor is introduced, S-LSR can operate satisfying the maintenance condition for the crystalline beam, in addition to the state free from the shear heating induced by dispersion. As the practical method to realize the dispersion suppressor including the electric field of the field index 0, we have suggested using a cylindrical electrostatic deflector equipped with intermediate electrodes. The electric field distribution of the field index 0 has been realized approxi-

mately by adjusting the applied voltage to the intermediate electrodes. It has been shown that the ring can accumulate an adequate beam current for the experiment generating the crystalline beams at the operating point $(\nu_x, \nu_y) = (2.072, 2.072)$, although the nonlinearity of the dispersion suppressor limits the dynamic aperture. It has been estimated that the size of the beam becomes far smaller compared to the dynamic aperture in the final state of the cooling. When the line density of the beam is low, it is thought that the beam reaches the crystalline state, at the operating point $(\nu_x, \nu_y) = (2.072, 2.072)$ of S-LSR. Once the crystalline beam is formed, the structure is thought to be maintained stably since this operating point satisfies the maintenance condition and nonlinear effects are negligible. However, as the line density of the beam increases, in the cooling process, the blocking of the emittance reduction induced by the second-order coherent resonance which originates in the lattice structure becomes remarkable [31]. The search of the maximum crystalline structure which can crystallize will be the main subject of our next investigation. This will be studied by a molecular dynamics simulation and experiments in the "dispersion-free storage ring S-LSR."

ACKNOWLEDGMENTS

The authors would like to present their thanks to Dr. H. Okamoto for the construction of the basis of the Hamiltonian formalism of the dispersion suppressor. One of the authors (M. Ikegami) thanks Dr. H. Fadil for helpful discussions.

APPENDIX A: SOLUTIONS OF THE MAXWELL EQUATION

In the space between the deflection electrodes, the scalar potential of the electric field ϕ has to be the solutions of the Laplace equation.

$$\Delta \phi = 0. \quad (\text{A1})$$

In a polar coordinate system (ρ, θ, φ) , the elemental solutions of the Laplace equation are represented as

$$\begin{aligned} \phi(\rho, \theta, \varphi) &= a_{ml} \rho^m Y_m^l(\theta, \varphi), \\ \phi(\rho, \theta, \varphi) &= \frac{b_{ml}}{\rho^{m+1}} Y_m^l(\theta, \varphi), \end{aligned} \quad (\text{A2})$$

where m is zero or a positive integer, $Y_m^l(\theta, \varphi)$ is a spherical harmonic, $l = -m, -m + 1, \dots, m - 1, m$, and a_{ml}, b_{ml} are constants. The usable electrostatic potential for electrostatic deflectors must have axial symmetry, at least. Therefore, the solutions must not have φ dependence. When the axial symmetry condition is imposed, the solutions become

$$\begin{aligned}\phi(\rho, \theta, \varphi) &= a_m \rho^m P_m(\cos\theta), \\ \phi(\rho, \theta, \varphi) &= \frac{b_m}{\rho^{m+1}} P_m(\cos\theta),\end{aligned}\quad (\text{A3})$$

where P_m is the Legendre polynomial.

Next, we transform the solutions Eq. (A3), to a cylindrical coordinate system. The relations between the polar coordinates and cylindrical coordinates (r, φ, z) are given by

$$\rho = \sqrt{r^2 + z^2} \quad \varphi = \varphi \quad \cos\theta = \frac{z}{\sqrt{r^2 + z^2}}. \quad (\text{A4})$$

Then, for $m = 0, 1, 2, \dots$ we obtain the following solutions

$$m = 0 \quad \phi(r, \varphi, z) = a_0, \quad (\text{A5})$$

$$\phi(r, \varphi, z) = \frac{b_0}{\sqrt{r^2 + z^2}}, \quad (\text{A6})$$

$$m = 1 \quad \phi(r, \varphi, z) = a_1 z, \quad (\text{A7})$$

$$\phi(r, \varphi, z) = \frac{b_1 z}{(r^2 + z^2)^{3/2}}, \quad (\text{A8})$$

$$m = 2 \quad \phi(r, \varphi, z) = a_2 (r^2 - 2z^2), \quad (\text{A9})$$

$$\phi(r, \varphi, z) = \frac{b_2 (r^2 - 2z^2)}{(r^2 + z^2)^{5/2}}. \quad (\text{A10})$$

...

The usable electric field as the bending electrostatic deflector must have a radial component (r component), and must not have vertical component (z component) on the median plane, and the electrostatic potential should be symmetric about z . Therefore, Eqs. (A7) and (A8) cannot be used as the bending electrostatic deflectors. Eventually, only the electrostatic potentials of even numbers of m can be used. In addition to the above solutions, a solution satisfying the condition for electrostatic deflector exists. That is a cylindrical electrostatic potential.

$$\phi(r, \varphi, z) = a \cdot \ln(r). \quad (\text{A11})$$

This solution can be obtained easily in the cylindrical coordinate system, under axial symmetry.

The linear combinations of the above solutions are also the solutions of the Laplace equation, and generate the usable electrostatic field.

When a circle of the radius ρ_0 in the cylindrical coordinate system is selected as the reference orbit of the Frenet-Serret coordinate system, the relations between the cylindrical coordinates and the Frenet-Serret coordinates are given by

$$\rho_0 + x = r \quad s = \rho_0 \varphi \quad y = z. \quad (\text{A12})$$

When these notations are used, for example, the linear combinations of the solutions Eq. (A5) and Eqs. (A6), (A9), and (A11) are represented as

$$\phi_{2D}(x, y, s) = V_0 \left[1 - \frac{1}{\sqrt{(1 + x/\rho_0)^2 + (y/\rho_0)^2}} \right], \quad (\text{A13})$$

$$\phi_{1D}(x, y, s) = V_0 \ln\left(1 + \frac{x}{\rho_0}\right), \quad (\text{A14})$$

$$\phi_{-1D}(x, y, s) = \frac{V_0}{2} \left[\left(1 + \frac{x}{\rho_0}\right)^2 - 2\left(\frac{y}{\rho_0}\right)^2 - 1 \right], \quad (\text{A15})$$

where the constant terms have been selected so that the electrostatic potential is 0 and the strength of the electric field is V_0/ρ_0 , on the reference orbit. These are spherical, cylindrical and hyperboloidal electrostatic potential. The field indices of these electric fields are 2, 1, and -1 , respectively. The electric fields which have larger field indices are realized, when the value of m in Eq. (A3) is selected to larger integer. An arbitrary real number field index is created by the linear combination of the above linearly independent electrostatic potentials. If an arbitrary electrostatic potential composed of the linear combination of the above electrostatic potentials are expanded in power series of x and y , it always becomes to the form of Eq. (5).

As an example, we show the shape of the electrodes generating electric fields which have the field index of the

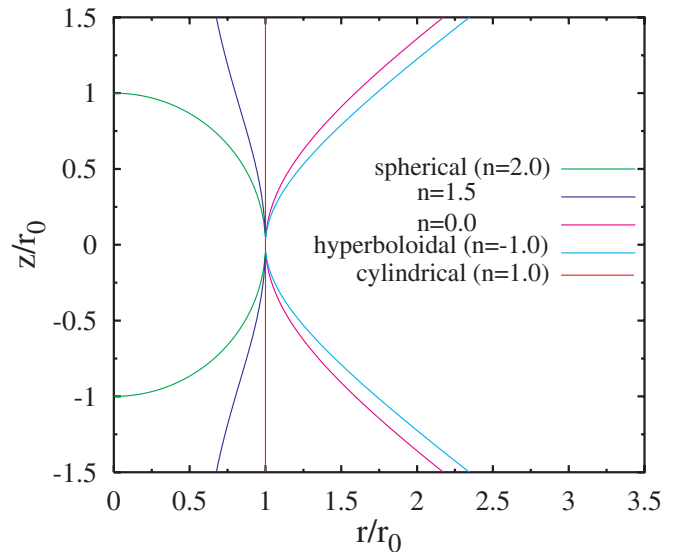


FIG. 7. (Color) Cross sectional shapes of various electrodes in the r - z plane of the cylindrical coordinate system. The shapes of the electrodes are equal potential curve. The variables have been scaled by the curvature radius of the electrode r_0 on the horizontal plane. The constant terms of each electrode has been selected so that the electrodes cross at the point $(r/r_0, z/r_0) = (1, 0)$.

value between 2 and -1 (Fig. 7). The shape of the electrode is decided by equal potential surface. Toroidal electrostatic deflectors can generate various field distributions [16]. They give the same linear focusing as the deflectors shown in Fig. 7 under the paraxial approximation.

APPENDIX B: TRANSFORMATION OF VARIABLES

A canonical transformation from $(x, \tilde{p}_x, y, \tilde{p}_y, t, p_t/p_0)$ to $(x, \tilde{p}_x, y, \tilde{p}_y, -c\Delta t, \Delta E/cp_0)$ is considered. When the Hamiltonian Eq. (7) is divided by the reference momentum p_0 , the canonical equations for $(t, p_t/p_0)$ become

$$\frac{dt}{ds} = \frac{\partial \hat{H}}{\partial \hat{p}_t}, \quad (\text{B1})$$

$$\frac{d\hat{p}_t}{ds} = -\frac{\partial \hat{H}}{\partial t}, \quad (\text{B2})$$

where $\hat{p}_t = p_t/p_0$, $\hat{H} = H/p_0$.

Using the relation $p_t = -E$, Eq. (B1) is rewritten to

$$\frac{d(ct)}{ds} = -\frac{\partial \hat{H}}{\partial (E/cp_0)}. \quad (\text{B3})$$

When the relation $\Delta E/cp_0 = E/cp_0 - 1/\beta_0$ is used, the Hamiltonian becomes

$$\begin{aligned} \hat{H} = & -\left(1 + \frac{x}{\rho_0}\right) \\ & \times \sqrt{1 + \frac{2}{\beta_0} \left(\frac{\Delta E - q\phi_D}{cp_0}\right) + \left(\frac{\Delta E - q\phi_D}{cp_0}\right)^2} - \tilde{p}_x^2 - \tilde{p}_y^2 \\ & - \left(1 + \frac{x}{\rho_0}\right) \frac{qA_s}{p_0}. \end{aligned} \quad (\text{B4})$$

Since the Hamiltonian does not depend on the time t explicitly, from Eq. (B2), the following relation is obtained:

$$\frac{d}{ds} \left(\frac{\Delta E}{cp_0} \right) = 0. \quad (\text{B5})$$

Furthermore, when the relations $s = c\beta_0 t_0$, $\Delta t = t - t_0$ and

$$\begin{aligned} & \frac{\partial}{\partial (\Delta E/cp_0)} \hat{H}(x, \tilde{p}_x, y, \tilde{p}_y, -c\Delta t, \Delta E/cp_0) \\ & = \frac{\partial}{\partial (E/cp_0)} \hat{H}(x, \tilde{p}_x, y, \tilde{p}_y, t, -E/p_0) \end{aligned} \quad (\text{B6})$$

are used, Eq. (B3) becomes

$$\begin{aligned} \frac{d(-c\Delta t)}{ds} & = \frac{1}{\beta_0} - \frac{d(ct)}{ds} = \frac{1}{\beta_0} + \frac{\partial \hat{H}}{\partial (\Delta E/cp_0)} \\ & = \frac{\partial}{\partial (\Delta E/cp_0)} \left(\hat{H} + \frac{1}{\beta_0} \frac{\Delta E}{cp_0} \right). \end{aligned} \quad (\text{B7})$$

Therefore, for the canonical variables $(-c\Delta t, \Delta E/cp_0)$, the Hamiltonian is rewritten as

$$\tilde{H} = \hat{H} + \frac{1}{\beta_0} \frac{\Delta E}{cp_0}. \quad (\text{B8})$$

The above transformation can be summarized by a canonical transformation

$$-c\Delta t = \frac{s}{\beta_0} - ct \quad \frac{\Delta E}{cp_0} = \frac{E}{cp_0} - \frac{1}{\beta_0}, \quad (\text{B9})$$

which is generated by the following generating function:

$$\begin{aligned} W(x, \tilde{p}_x, y, \tilde{p}_y, t, \Delta E/cp_0) = & \left(\frac{s}{\beta_0} - ct \right) \frac{\Delta E}{cp_0} - \frac{ct}{\beta_0} \\ & + \tilde{p}_x x + \tilde{p}_y y. \end{aligned} \quad (\text{B10})$$

The transformation of $(x, \tilde{p}_x, y, \tilde{p}_y)$ is an identical transformation. This generating function is equivalent to the generating function defined in Ref. [27]. It is obtained by the same way as the method shown in Ref. [33].

APPENDIX C: THIRD-ORDER HAMILTONIAN, LIE TRANSFORMATION, AND THE COEFFICIENTS OF SECOND-ORDER TRANSPORT EQUATION

In this appendix, the canonical variable $\Delta E/cp_0$ is replaced by δ , in order to simplify the notation.

When the Hamiltonian Eq. (9) is expanded up to the third order of the canonical variables $v_i \equiv (x, \tilde{p}_x, y, \tilde{p}_y, -c\Delta t, \delta)$, the second-order terms are

$$\begin{aligned} \tilde{H}_2(v_i) = & \frac{1}{2\gamma_0^2} \left(\frac{\delta}{\beta_0} \right)^2 + \frac{\tilde{p}_x^2 + \tilde{p}_y^2}{2} - \frac{\delta}{\beta_0} \frac{x}{\rho_0} \left(1 - \frac{qV_0}{\gamma_0^2 \beta_0^2 E_0} \right) \\ & + \frac{1}{2} \left[1 - (1-n) \frac{qV_0}{\beta_0^2 E_0} + \frac{1}{\gamma_0^2} \left(\frac{qV_0}{\beta_0^2 E_0} \right)^2 \right] \left(\frac{x}{\rho_0} \right)^2 \\ & + \frac{1}{2} (1-n) \frac{qV_0}{\beta_0^2 E_0} \left(\frac{y}{\rho_0} \right)^2 \end{aligned} \quad (\text{C1})$$

and the third-order terms are

$$\begin{aligned}
\tilde{H}_3(v_i) = & -\frac{1}{2}\left(\frac{\delta}{\beta_0}\right)\left[\tilde{p}_x^2 + \tilde{p}_y^2 + \frac{1}{\gamma_0^2}\left(\frac{\delta}{\beta_0}\right)^2\right] + \frac{1}{2}\left(\frac{x}{\rho_0}\right)^3\left[\left(n - \frac{K_2}{3}\right)\frac{qV_0}{\beta_0^2 E_0} + \frac{1}{\gamma_0^2}(1-n)\left(\frac{qV_0}{\beta_0^2 E_0}\right)^2 - \frac{1}{\gamma_0^2}\left(\frac{qV_0}{\beta_0^2 E_0}\right)^3\right] \\
& + \frac{1}{2\gamma_0^2}\left(\frac{x}{\rho_0}\right)^2\left(\frac{\delta}{\beta_0}\right)\left[(2-n)\frac{qV_0}{\beta_0^2 E_0} - 3\left(\frac{qV_0}{\beta_0^2 E_0}\right)^2\right] + \frac{1}{2\gamma_0^2}\left(\frac{y}{\rho_0}\right)^2\left(\frac{\delta}{\beta_0}\right)\left(\frac{qV_0}{\beta_0^2 E_0}\right)(n-1) + \frac{x}{\rho_0}\left\{\frac{\tilde{p}_x^2 + \tilde{p}_y^2}{2}\left(1 - \frac{qV_0}{\beta_0^2 E_0}\right)\right. \\
& \left. + \frac{1}{2\gamma_0^2}\left(1 - 3\frac{qV_0}{\beta_0^2 E_0}\right)\left(\frac{\delta}{\beta_0}\right)^2 + \frac{1}{2}\left(\frac{y}{\rho_0}\right)^2\left(\frac{qV_0}{\beta_0^2 E_0}\right)\left[K_2 - 2n + (n-1)\frac{1}{\gamma_0^2}\frac{qV_0}{\beta_0^2 E_0}\right]\right\}. \quad (C2)
\end{aligned}$$

In Ref. [34] it is shown that the third-order Lie polynomial is given by

$$\begin{aligned}
F_3 = & -\sum_{k=1}^6 \int_0^L \tilde{H}_3[R_{ik}^{-1}(s)v_k]ds \\
\equiv & \sum_{i=1}^6 \sum_{j=1}^6 \sum_{k=1}^6 F_{ijk}v_i v_j v_k / 3! \quad (C3)
\end{aligned}$$

where R_{ik}^{-1} is the component of the inverse matrix of the transfer matrix.

The coefficients of this polynomial have the following symmetry:

$$F_{ijk} = F_{ikj} = F_{jik} = F_{jki} = F_{kji} = F_{kij}. \quad (C4)$$

By using the coefficients of the Lie polynomial, the coefficients of the second-order transport equation T_{ijk} are obtained from the following formula :

$$T_{ijk} = \frac{(-1)^i}{2} \sum_{m=1}^6 \sum_{n=1}^6 F_{(i+(-1)^{i+1})mn} R_{mj} R_{nk}. \quad (C5)$$

-
- [1] A. Rahman and J.P. Schiffer, Phys. Rev. Lett. **57**, 1133 (1986).
[2] J. Wei, X.-P. Li, and A.M. Sessler, Phys. Rev. Lett. **73**, 3089 (1994).
[3] J. Wei, X.-P. Li, and A.M. Sessler, in *Advanced Accelerator Concepts, Proceedings of the Sixth Advanced Accelerator Concepts Workshop, Fontana, 1994*, edited by P. Schoessow, AIP Conf. Proc. No. 335 (AIP, New York, 1995).
[4] J. Wei, H. Okamoto, and A.M. Sessler, Phys. Rev. Lett. **80**, 2606 (1998).
[5] H. Okamoto, A.M. Sessler, D. Möhl, Phys. Rev. Lett. **72**, 3977 (1994).
[6] H. Okamoto, Phys. Rev. E **50**, 4982 (1994).
[7] T. Kihara, H. Okamoto, Y. Iwashita, K. Oide, G. Lamanna, and J. Wei, Phys. Rev. E **59**, 3594 (1999).
[8] Y. Yuri and H. Okamoto, Phys. Rev. Lett. **93**, 204801 (2004).
[9] H. Okamoto and J. Wei, Phys. Rev. E **58**, 3817 (1998).
[10] H. Okamoto, Nucl. Instrum. Methods Phys. Res., Sect. A **532**, 32 (2004).
[11] R.E. Pollock, Z. Phys. A **341**, 95 (1991).
[12] W. Henneberg, Ann. Phys. (Leipzig) **19**, 335 (1934).

- [13] W.E. Millet, Phys. Rev. **74**, 1058 (1948).
[14] M. Ikegami, A. Noda, M. Tanabe, M. Grieser, and H. Okamoto, Phys. Rev. ST Accel. Beams **7**, 120101 (2004).
[15] A. Noda, Nucl. Instrum. Methods Phys. Res., Sect. A **532**, 150 (2004).
[16] *Focusing of Charged Particles*, edited by A. Septier (Academic Press, New York, 1967).
[17] S.P. Møller and U.V. Pedersen, in *Proceedings of the 7th European Particle Accelerator Conference, EPAC2000, Vienna* (EPS, Geneva, 2000), p. 794.
[18] S.P. Møller, Nucl. Instrum. Methods Phys. Res., Sect. A **394**, 281 (1997).
[19] T. Tanabe, K. Chida, K. Noda, and I. Watanabe, Nucl. Instrum. Methods Phys. Res., Sect. A **482**, 595 (2002).
[20] F.C. Iselin, Part. Accel. **17**, 143 (1985).
[21] S.Y. Lee, *Accelerator Physics* (World Scientific, Singapore, 1999), p. 30. The notation of the present paper is consistent with this reference, when the vertical coordinate y and the components of the vector potential A_s, A_y are replaced by $-z$ and $A_2, -A_3$, respectively.
[22] S. Jinno, T. Takao, Y. Omata, A. Satou, H. Tanuma, T. Azuma, H. Shiromaru, K. Okuno, N. Kobayashi, and I. Watanabe, Nucl. Instrum. Methods Phys. Res., Sect. A **532**, 477 (2004).
[23] R. von Hahn, J. Crespo López-Urrutia, M. Grieser, D. Orlov, C.D. Schröter, D. Schwalm, J. Ullrich, C.P. Welsch, A. Wolf, Daniel Zajfman, and X. Urbain, in *Proceedings of the 9th European Particle Accelerator Conference (EPAC2004), Lucerne, 2004* (EPS-AG, Lucerne, 2003), p. 1237.
[24] Reference [21], p. 37.
[25] K.L. Brown and R.V. Servranckx, Report No. SLAC-PUB-3381, p. 15.
[26] H. Okamoto and S. Machida, Nucl. Instrum. Methods Phys. Res., Sect. A **482**, 65 (2002).
[27] The transfer matrix calculation was performed, using the code MAD8. Refer to the following about the calculation method: H. Grote and F.C. Iselin, *The Mad Program User's Reference Manual*, Report No. CERN/SL/90-13, 1996: <http://hansg.home.cern.ch/hansg/mad/mad8/mad8.html>; F.C. Iselin, *The Mad Program Physical Method Manual*, Report No. CERN/SL/92, 1994, p. 16: <http://hansg.home.cern.ch/hansg/mad/mad8/mad8.html>.
[28] M. Ikegami, M. Tanabe, T. Shirai, H. Tongu, K. Noda, M. Grieser, and A. Noda, Nucl. Instrum. Methods Phys. Res., Sect. A **532**, 492 (2004).
[29] M. Ikegami, dissertation, Kyoto-University, 2005.

- [30] M. Tanabe, M. Ikegami, A. Noda, T. Shirai, H. Souda, H. Tongu, S. Shibuya, and K. Noda, in Proceedings of the International Workshop on Beam Cooling and Related Topics COOL 05 (to be published).
- [31] K. Okabe and H. Okamoto, *Jpn. J. Appl. Phys.* **42**, 4584 (2003).
- [32] R. W. Hasse and J. P. Schiffer, *Ann. Phys. (N.Y.)* **203**, 419 (1990).
- [33] T. Suzuki, *Part. Accel.* **12**, 237 (1982).
- [34] D. R. Douglas, Doctoral thesis, University of Maryland, 1982.